Driver Parameter Estimation Using Joint E-/UKF and Dual E-/UKF Under Nonlinear State Inequality Constraints

Changxi You
School of Aerospace Engineering
Georgia Institute of Technology
Atlanta, GA 30332–0150, USA
Email: cyou6@gatech.edu

Jianbo Lu
Research & Advanced Engineering
Ford Motor Company
Dearborn. MI 48121, USA.
Email: jlu10@ford.com

Panagiotis Tsiotras
School of Aerospace Engineering
Georgia Institute of Technology
Atlanta, GA 30332–0150, USA
Email: tsiotras@gatech.edu

***Abstract*—In the development of advanced driver-assist systems (ADAS) for lane-keeping, one important design objective is to appropriately share the steering control with the driver. Hence, the steering behavior of the driver must be well known beforehand. This paper adopts the well-known two-point visual driver model to characterize the steering behavior of the driver, and conducts a series of field tests to identify the model parameters to validate the two-point visual driver model in real scenarios. Both an extended Kalman filter and an unscented Kalman filter are implemented for estimating the unknown driver parameters, using a joint-state estimation algorithm and a dual estimation algorithm, and the results are compared.**

I. INTRODUCTION

Driver modeling is an important part of modern, semi-autonomous driver-vehicle-road systems [1], [2]. In order to characterize driver behavior, researchers have proposed different driver models based on several methodologies over the past decades [3], [4], [5], [6].

This paper adopts the two-point driver model from [7], which combines both the two-level visual strategy and the high-frequency kinesthetic feedback of the driver that accounts for the interaction between the driver's arms and the steering wheel [4]. The two-point driver model is derived from the concept of the two-level steering mechanism [8], [9]. In [8] Donges divided the driver's steering task into a guidance level and a stabilization level, and thereby built a two-level steering model. The guidance level interprets driver's perception and response with respect to the oncoming road in an anticipatory open-loop control fashion. The stabilization level interprets the driver's compensatory behavior with respect to the deviation from the reference path in a closed-loop control mode. This idea has been widely accepted and has been further developed by subsequent researchers, such as [9], [10], [7], [11].

Although some work has been done to validate the two point driver model and identify the driver parameters using a simulator [7], it is still necessary to validate the model using actual, field test data, especially when an effective identification method is to be developed with the requirement to work on line on commercial vehicles. This paper assumes that all parameters of the driver model are identifiable, and compares four methods — the joint E-/UKF and the dual E-/UKF [12] — to estimate the driver model parameters. The methods are validated against both simulation data and against data collected through a series of field tests.

978-1-5090-1897-0/16/$31.00

II. SYSTEM MODELING AND PROBLEM FORMULATION

The proposed driver-vehicle-road system consists of four subsystems, as shown in Fig. 1: the driver model, the steering column model, the vehicle model and the road and perception model. The input to the system is the curvature of the road ρ_{ref}. The primary performance variable is the lateral deviation of the so-called "near point" directly in front of the vehicle from to the centerline of road, Δy (see Fig. 1).

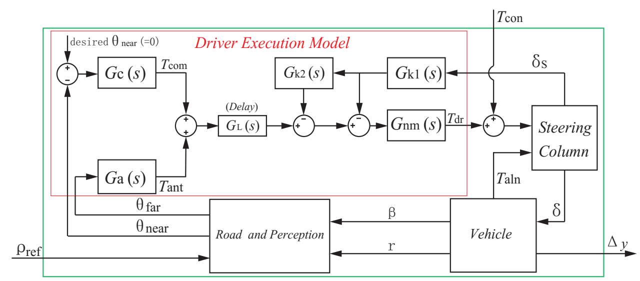

Fig. 1. Human-vehicle-road closed-loop system.

A. Driver Model

In this paper we use the driver model initially proposed in [7] and also used in [13].The structure of this model is shown in the red rectangular box in Fig. 1. The transfer functions $G_{\mathrm{a}}(s)$ and $G_{\mathrm{c}}(s)$ account for the anticipatory control and the compensatory control actions of the driver, respectively. The system $G_{\mathrm{nm}}(s)$ approximately describes the neuromuscular response of the driver's arms. The "$Delay$" block indicates the driver's processing delay in the brain and $G_{\mathrm{k1}}(s)$ and $G_{\mathrm{k2}}(s)$ account for the driver's kinesthetic perception of the steering system. T_{ant} and T_{com} denote the driver's steering torques corresponding to the anticipatory control and the compensatory control paths, respectively; δ_{s} denotes the steering wheel angle; and the inputs θ_{near} and θ_{far} denote the near field and the far field visual angles, respectively (see Fig. 2). Finally, T_{dr} denotes the driver's total steering torque delivered to the steering wheel. The transfer functions of the blocks are given below

$$G_{\mathrm{a}}(s) = K_{\mathrm{a}}, \quad G_{\mathrm{c}}(s) = K_{\mathrm{c}}\frac{T_{\mathrm{L}}s+1}{T_{\mathrm{I}}s+1}, \quad G_{\mathrm{k_1}}(s) = K_{\mathrm{D}}\frac{T_{\mathrm{k_1}}s}{T_{\mathrm{k_1}}s+1},$$

$$G_{\mathrm{L}}(s) = e^{-t_{\mathrm{p}}s}, \quad G_{\mathrm{nm}}(s) = \frac{1}{T_{\mathrm{N}}s+1}, \quad G_{\mathrm{k_2}}(s) = K_{\mathrm{G}}\frac{T_{\mathrm{k_2}}s+1}{T_{\mathrm{k_3}}s+1},$$

where $K_{\rm a}$ and $K_{\rm c}$ are static gains for the anticipatory and compensatory control subsystems, respectively; $K_{\rm D}$ and $K_{\rm G}$ are static gains for the kinesthetic perception feedback subsystems, respectively; $T_{\rm L}$ and $T_{\rm I}$ ($T_{\rm L} > T_{\rm I}$) are the lead time and lag time constants, respectively; $T_{\rm k_1}$, $T_{\rm k_2}$ and $T_{\rm k_3}$ are the three time constants of the driver's kinesthetic perception feedback from the steering wheel, $t_{\rm p}$ is the delay for the driver to process sensory signals and $T_{\rm N}$ is the time constant of the driver's arm neuromuscular system. The mathematical model of the driver subsystem is then formulated as

$$\dot{x}_{\rm d} = A_{\rm d}x_{\rm d} + B_{\rm d}u_{\rm d}, \tag{1a}$$

$$y_{\rm d} = C_{\rm d}x_{\rm d} + D_{\rm d}u_{\rm d}, \tag{1b}$$

where the input is $u_{\rm d} = (\theta_{\rm near}, \theta_{\rm far}, \delta_{\rm s})^{\rm T}$ and the output is $y_{\rm d} = T_{\rm dr} = T_{\rm dr}^{\rm ff} + T_{\rm dr}^{\rm fb}$, where $T_{\rm dr}^{\rm ff}$ and $T_{\rm dr}^{\rm fb}$ denote the two components of the driver's steering torque, resulting from the feedforward path and the feedback path, respectively.

B. Road and Perception Model

The road and perception model interacts with both the vehicle model and the driver model (refer to Fig. 1) and achieves two functions: (a) it determines the vehicle's position and posture relative to the road geometry; and (b) it determines the location of the driver's near and far visual points on the upcoming road. In Fig. 2 the frame $\rm X_I$-O-$\rm Y_I$ is fixed on the road. It is assumed that the vehicle is cornering with a certain lateral deviation from the road centerline. Let ψ denote the vehicle's yaw angle, let $\psi_{\rm t}$ denote the angle between the tangent to the road centerline and the $\rm X_I$ axis, and let M denote the current position of the vehicle's center of mass. Let also A denote the driver's "lookahead" point in front of M at a distance $\ell_{\rm s}$ along the vehicle's heading direction, B denote the intersection of OA with the road centerline, and let C denote the point of tangency of the line along the gaze direction on the road's inner boundary. Furthermore, let $L_{\rm s}$ denote the distance between C and M, $\theta_{\rm far}$ denote the far point visual angle between the gaze direction of the driver and the heading direction of the vehicle, $\theta_{\rm near}$ denote the near point visual angle between MB and the heading direction of the vehicle. Finally, in Fig. 2 Δy denotes the length of the line segment AB, $R_{\rm ref}$ denotes the radius of the road's inner boundary, d denotes the distance from M to the road's inner boundary, and D denotes the width of the road. Henceforth, it will be assumed that d and D are small compared to $R_{\rm ref}$.

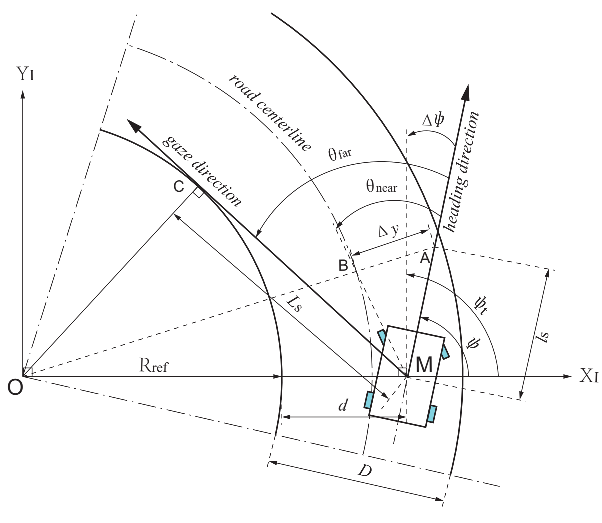

Fig. 2. Road geometries, vehicle states and driver's visual perception.

From Fig. 2, the near and far distance visual perception angles can be approximated as [8], [7]

$$\theta_{\rm near} \approx \frac{\Delta y}{\ell_{\rm s}}, \qquad \theta_{\rm far} \approx \frac{L_{\rm s}}{R_{\rm ref}} + \Delta\psi \approx L_{\rm s}\rho_{\rm ref} + \Delta\psi,$$

where $\rho_{\rm ref} = 1/R_{\rm ref}$ is the road curvature, and $\Delta\psi = \psi_{\rm t} - \psi$ is the angle difference between the tangent of the road centerline and the vehicle's heading direction. It can be directly shown that Δy and $\Delta\psi$ obey the following equations:

$$\Delta\dot{y} = -V_{\rm x}(\beta - \Delta\psi) - \ell_{\rm s}r + V_{\rm x}\ell_{\rm s}\rho_{\rm ref}, \qquad \Delta\dot{\psi} = \dot{\psi}_{\rm t} - r,$$

where β is the vehicle sideslip angle and r is the yaw rate. Furthermore, since $\dot{\psi}_{\rm t}$ can be approximated by $V_{\rm x}\rho_{\rm ref}$, it follows that $\Delta\dot{\psi} = V_{\rm x}\rho_{\rm ref} - r$. Therefore, the road and perception system can be formulated as

$$\dot{x}_{\rm r} = A_{\rm r}x_{\rm r} + B_{\rm r}u_{\rm r}, \tag{2a}$$

$$y_{\rm r} = C_{\rm r}x_{\rm r} + D_{\rm r}u_{\rm r}, \tag{2b}$$

where $x_{\rm r} = (\Delta\psi, \Delta y)^{\rm T}$, $u_{\rm r} = (\rho_{\rm ref}, \beta, r)^{\rm T}$ and $y_{\rm r} = (\Delta\psi, \Delta y, \theta_{\rm near}, \theta_{\rm far})^{\rm T}$. We use the same steering column model and the same vehicle model as in [13].

C. Problem Formulation

For notational simplicity, let $p_1 = K_{\rm a}$, $p_2 = K_{\rm c}$, $p_3 = T_{\rm L}$, $p_4 = T_{\rm I}$, $p_5 = T_{\rm N}$, $p_6 = t_{\rm p}$ and $p_7 = \ell_{\rm s}$. We further let $p_8 = K_{\rm D}$, $p_9 = K_{\rm G}$, $p_{10} = T_{\rm k_1}$, $p_{11} = T_{\rm k_2}$ and $p_{12} = T_{\rm k_3}$ for the high frequency kinesthetic feedback in the driver model. Since the human driver has physical limits, each model parameter is restricted to lie within some compact interval, $p_i \in [\underline{p_i},\ \overline{p_i}]$, $i = 1, 2, \ldots, 12$. Let $p = (p_1,\ p_2, \ldots,\ p_{12})^{\rm T} \in \mathbb{R}^{12}$, and let $\mathcal{P} = [\underline{p_1}, \overline{p_1}] \times [\underline{p_2}, \overline{p_2}] \times \cdots \times [\underline{p_{12}}, \overline{p_{12}}] \subset \mathbb{R}^{12}$.

We consider the combined system of the driver model in (1) and the road and perception model in (2),

$$\dot{x}^{\rm c} = A^{\rm c}(p)x^{\rm c} + B^{\rm c}(p)u^{\rm c}, \tag{3a}$$

$$y^{\rm c} = C^{\rm c}x^{\rm c}, \tag{3b}$$

where the input is $u^{\rm c} = (\rho, \beta, r, \delta_{\rm s})^{\rm T}$ and the output is $y^{\rm c} = T_{\rm dr}^{\rm ff} + T_{\rm dr}^{\rm fb}$. Assuming we can measure $u^{\rm c}$ and $y^{\rm c}$, we can use state estimation techniques to identify the driver parameter vector p in (3a)-(3b). To this end, we define an alternative parameter vector $\nu = (\nu_1, \nu_1, \ldots, \nu_{12})$ as follows

$$\begin{aligned}
&\nu_1 = \frac{1}{p_4}, \quad \nu_2 = \frac{1}{p_6}, \quad \nu_3 = \frac{1}{p_5}, \quad \nu_4 = \frac{p_1}{p_5}, \\
&\nu_5 = \frac{p_2 p_3}{p_4 p_6 p_7}, \quad \nu_6 = \frac{p_2}{p_4 p_7}, \quad \nu_7 = p_7, \quad \nu_8 = p_8, \\
&\nu_9 = p_9, \quad \nu_{10} = \frac{1}{p_{10}}, \quad \nu_{11} = p_{11}, \quad \nu_{12} = \frac{1}{p_{12}}.
\end{aligned} \tag{4}$$

$$
\left[\begin{array}{c|c} A^{\mathrm{c}}(\nu) & B^{\mathrm{c}}(\nu) \\ \hline C^{\mathrm{c}} & 0 \end{array}\right] = \left[\begin{array}{cccccccc|cccc}
0 & 0 & 0 & 0 & 0 & 0 & 0 & 0 & V_{\mathrm{x}} & 0 & -1 & 0 \\
V_{\mathrm{x}} & 0 & 0 & 0 & 0 & 0 & 0 & 0 & V_{\mathrm{x}}\nu_7 & -V_{\mathrm{x}} & -\nu_7 & 0 \\
0 & \nu_6 - \frac{\nu_1\nu_5}{\nu_2} & -\nu_1 & 0 & 0 & 0 & 0 & 0 & 0 & 0 & 0 & 0 \\
4\frac{\nu_2\nu_4}{\nu_3} & 4\nu_5 & 4\nu_2 & -2\nu_2 & 0 & 0 & 0 & 0 & 4\frac{L_{\mathrm{s}}\nu_2\nu_4}{\nu_3} & 0 & 0 & 0 \\
-\nu_4 & -\nu_5 & -\nu_3 & \nu_3 & -\nu_3 & 0 & 0 & 0 & -L_{\mathrm{s}}\nu_4 & 0 & 0 & 0 \\
0 & 0 & 0 & 0 & 0 & 0 & 0 & -\nu_3\nu_{10}\nu_{12} & 0 & 0 & 0 & 0 \\
0 & 0 & 0 & 0 & 0 & 1 & 0 & -\nu_3\nu_{10} - \nu_3\nu_{12} - \nu_{10}\nu_{12} & 0 & 0 & 0 & -\nu_3\nu_8\nu_{12}(\nu_9 + 1) \\
0 & 0 & 0 & 0 & 0 & 0 & 1 & -\nu_3 - \nu_{10} - \nu_{12} & 0 & 0 & 0 & -\nu_3\nu_8(\nu_9\nu_{11}\nu_{12} + 1) \\ \hline
0 & 0 & 0 & 0 & 1 & 0 & 0 & 1 & 0 & 0 & 0 & 0
\end{array}\right]. \tag{5}
$$

Then the system matrices in (3) are given by equation (5). If we let Δt denote the sampling interval and discretize the system in (3), we obtain the following discrete system subject to noise

$$x^{\mathrm{c}}_{k+1} = A^{\mathrm{c}}_{\mathrm{D}}(\nu)x^{\mathrm{c}}_k + B^{\mathrm{c}}_{\mathrm{D}}(\nu)u^{\mathrm{c}}_k + w_k, \tag{6a}$$
$$y^{\mathrm{c}}_k = C^{\mathrm{c}}_{\mathrm{D}}x^{\mathrm{c}}_k + v_k, \tag{6b}$$

where w_k and v_k are the process noise and the measure noise, respectively. In case of using the joint state E-/UKF for parameter identification, we include the parameter vector ν into the state vector and let $x = [x^{\mathrm{c}\,\mathrm{T}}, \nu^{\mathrm{T}}]^{\mathrm{T}}$. Recall that the parameter vector $p \in \mathcal{P}$. In the following sections we estimate the state vector of the system based on the available data (the input and the output), subject to the following constraints

$$\underline{p_i} \leqslant g_i(\nu) \leqslant \overline{p_i}, \qquad i = 1, 2, \ldots, 12, \tag{7}$$

where $g_i(\nu)$ is the ith element of the vector-valued function $g(\nu)$, which is given by

$$g(\nu) = [\ 1/\nu_1 \quad 1/\nu_2 \quad 1/\nu_3 \quad \nu_4/\nu_3 \quad \nu_5/(\nu_2\nu_6)$$
$$(\nu_6\nu_7)/\nu_1 \quad \nu_7 \quad \nu_8 \quad \nu_9 \quad 1/\nu_{10} \quad \nu_{11} \quad 1/\nu_{12}\ ]^{\mathrm{T}}. \tag{8}$$

The upper bounds and the lower bounds that define $\mathcal{P}$ are given in Table II. Note that, some of the parameters in the compensatory model, in particular in the neuromuscular system, can be considered as constants [4].

III. Parameter Estimation

In this section we use the joint E-/UKF and the dual E-/UKF to estimate the system states and obtain the driver parameters. The joint E-/UKF includes the unknown parameters into the original state vector and then estimates the new states. The dual E-/UKF separates the state space realizations of the original states and the parameters, so as to apply the Kalman filter to estimate the original states and the parameters separately.

A. *Extended Kalman Filter*

The EKF is one of the most common approaches to solve nonlinear estimation problems, by means of linearizing the nonlinear state transition models and the nonlinear observation models. The system states and the noise are assumed to be Gaussian random variables. For a system given in the following form,

$$x_{k+1} = f(x_k, u_k, w_k), \tag{9a}$$
$$y_k = h(x_k, u_k, v_k), \tag{9b}$$

where w_k and v_k are zero-means Gaussian process noise and measure noise, respectively, the EKF computes the estimations about the state and the covariance matrix using the following algorithm:

EKF Algorithm
1: Initialize with:
$\hat{x}_0 = \mathbb{E}[x_0]$
$\hat{P}_0 = \mathbb{E}[(x_0 - \hat{x}_0)(x_0 - \hat{x}_0)^{\mathrm{T}}]$
2: Prediction (time update):
$\hat{x}_k^- = f(\hat{x}_{k-1}, u_{k-1})$
$\hat{y}_k^- = h(\hat{x}_k^-, u_k)$
$\hat{P}_k^- = F_{k-1}\hat{P}_{k-1}F_{k-1}^{\mathrm{T}} + Q_w$
3: Measurement update:
$\epsilon_k = y_k - \hat{y}_k^-$
$S_k = H_k\hat{P}_k^- H_k^{\mathrm{T}} + Q_v$
$K_k = \hat{P}_k^- H_k^{\mathrm{T}} S_k^{-1}$
$\hat{x}_k = \hat{x}_k^- + K_k\epsilon_k$
$\hat{P}_k = \hat{P}_k^- - K_k S_k K_k^{\mathrm{T}}$

The matrix-valued functions F_{k-1} and H_k are the Jacobian matrices of $f(x, u)$ and $h(x, u)$, and are given by

$$F_{k-1} = \left.\frac{\partial f}{\partial x}\right|_{\hat{x}_{k-1}}, \qquad H_k = \left.\frac{\partial h}{\partial x}\right|_{\hat{x}_k^-}. \tag{10}$$

B. *Unscented Kalman Filter*

The UKF is based on the unscented transformation (UT). Hence, the UKF avoids calculating the Jacobian matrices at each time step, and captures the true mean and covariance of the state Gaussian random variable to at least second order accuracy (Taylor series expansion) for any nonlinearity. We consider an L-dimensional Gaussian random variable x with mean $\hat{x}$ and covariance P_x. To calculate the statistics of $y = g(x)$, we select $2L+1$ discrete sample points $\{\mathcal{X}_i\}_{i=0}^{2L}$ which are propagated through the system dynamics.

The UKF redefines the state vector as $x^a_k = [x_k^{\mathrm{T}}, w_k^{\mathrm{T}}, v_k^{\mathrm{T}}]^{\mathrm{T}}$, which concatenates the original state and the noise variables, and then estimates x^a_k recursively. The UKF equations are summarized in the following table, where λ is the principal scaling parameter, α determines the spread of sigma points around the mean $\hat{x}$ and is usually set to a small positive value (i.e., 1e-3), κ is a secondary scaling parameter which is usually set to 0 or $3-L$, and β is used to incorporate prior knowledge of the distribution of x. For Gaussian distribution, $\beta = 2$ is optimal [12]. $(\gamma\sqrt{P_x})_i$ is the ith column of the matrix square root.

UKF Algorithm

1: Initialize with:

$$\hat{x}_0 = \mathbb{E}[x_0]$$
$$P_0 = \mathbb{E}[(x_0 - \hat{x}_0)(x_0 - \hat{x}_0)^{\mathrm{T}}]$$
$$\hat{x}_0^a = \mathbb{E}[x_0^a] = [\hat{x}_0^{\mathrm{T}} \;\; 0 \;\; 0]^{\mathrm{T}}$$
$$P_0^a = \mathbb{E}[(x_0^a - \hat{x}_0^a)(x_0^a - \hat{x}_0^a)^{\mathrm{T}}] = \begin{bmatrix} P_0 & 0 & 0 \\ 0 & Q_w & 0 \\ 0 & 0 & Q_v \end{bmatrix}$$

2: Sigma-point calculation and prediction:

$$\mathcal{X}_{k-1}^a = [\hat{x}_{k-1}^a \quad \hat{x}_{k-1}^a + \gamma\sqrt{P_{k-1}^a} \quad \hat{x}_{k-1}^a - \gamma\sqrt{P_{k-1}^a}]$$
$$\mathcal{X}_{k|k-1}^x = f(\mathcal{X}_{k-1}^x, u_{k-1}, \mathcal{X}_{k-1}^w)$$
$$\hat{x}_k^- = \sum_{i=0}^{2L} W_i^{(m)} \mathcal{X}_{i,k|k-1}^x$$
$$P_k^- = \sum_{i=0}^{2L} W_i^{(c)} (\mathcal{X}_{i,k|k-1}^x - \hat{x}_k^-)(\mathcal{X}_{i,k|k-1}^x - \hat{x}_k^-)^{\mathrm{T}}$$
$$\mathcal{Y}_{k|k-1} = h(\mathcal{X}_{k|k-1}^x, u_{k-1}, \mathcal{X}_{k|k-1}^v)$$
$$\hat{y}_k^- = \sum_{i=0}^{2L} W_i^{(m)} \mathcal{Y}_{i,k|k-1}$$

3: Measurement update:

$$P_{y_k y_k} = \sum_{i=0}^{2L} W_i^{(c)} (\mathcal{Y}_{i,k|k-1} - \hat{y}_k^-)(\mathcal{Y}_{i,k|k-1} - \hat{y}_k^-)^{\mathrm{T}}$$
$$P_{x_k y_k} = \sum_{i=0}^{2L} W_i^{(c)} (\mathcal{X}_{i,k|k-1}^x - \hat{x}_k^-)(\mathcal{Y}_{i,k|k-1} - \hat{y}_k^-)^{\mathrm{T}}$$
$$\mathcal{K} = P_{x_k y_k} P_{y_k y_k}^{-1}$$
$$\hat{x}_k = \hat{x}_k^- + \mathcal{K}(y_k - \hat{y}_k^-)$$
$$P_k = P_k^- - \mathcal{K} P_{y_k y_k} \mathcal{K}^{\mathrm{T}}$$

Note: $x^a = [x^{\mathrm{T}} \;\; w^{\mathrm{T}} \;\; v^{\mathrm{T}}]^{\mathrm{T}}$, $\mathcal{X}^a = [(\mathcal{X}^x)^{\mathrm{T}} \;\; (\mathcal{X}^w)^{\mathrm{T}} \;\; (\mathcal{X}^v)^{\mathrm{T}}]^{\mathrm{T}}$.

C. *Nonlinear Inequality State Constraints*

The Kalman filtering constrained state estimation problem has been solved using a number of algorithms [14], [15], [16], [17]. In this study, we use the estimate projection algorithm and the first-order Taylor expansion approximation method [14] to solve the state estimation problem with nonlinear inequality constraints. Mathematically, we solve the following minimization problem

$$\tilde{x}_k = \underset{x}{\operatorname{argmin}} \;\; (x - \hat{x}_k)^{\mathrm{T}} W (x - \hat{x}_k), \tag{11a}$$
$$\text{such that} \quad g(x) \leqslant b, \tag{11b}$$

where $\hat{x}_k$ and $\tilde{x}_k$ are the unconstrained estimate and the constrained estimate of the state, respectively, and W is the weight matrix. We obtain the maximum probability estimate of the state subject to the state constraints when $W = P_k^{-1}$. If we perform a Taylor series expansion of (11b) around $\hat{x}(k)$ and ignore higher order terms, we obtain the linear approximation of the constraint inequalities in (11b),

$$g'(\hat{x}_k)x \leqslant b - g(\hat{x}_k) + g'(\hat{x}_k)\hat{x}_k. \tag{12}$$

The minimization problem of (11a) subject to the linear inequality constraints in (12) can be solved using a standard quadratic programming [5].

IV. Field Test

The field tests were conducted at the Ford Dearborn Development Center (DDC) test facility in November 2015. The Ford DDC is about 1,750 meters long from the West end to the East end and about 900 meters long from the South end to the North end. The width of the double-lane is about 6 meters. Three kinds of tests were conducted, namely, the steering handling course (SHC), the fixed-radius circling test (FRC) and the public road test (PRT). Three vehicles were used and the driving style of three types of the drivers were mimicked (see Fig. 3). Due to the lack of space, this paper only shows the results of the SHC tests, where the driver is an expert driver and the experimental vehicle is the MKS.

Fig. 3. Vehicles and apparatus used in the experiments. 1st row: Fiesta (left), MKS (medium), F150 (right); 2nd row: power source (left), power converter (medium), CAN case (right).

All data were collected through a vector CANcase connected to the OBD port of the vehicle, which transmits vehicle signals for HS-CAN and INFO-CAN, both of which have at a data rate of 500 [kB/s]. The HS-CAN connects to most of the regular on-board electronic control units (ECU), such as the anti-skip braking system (ABS), the electric power assisted steering (EPAS) system and the restraints control module (RCM). The INFO-CAN connects to the in-vehicle communications and entertainment system that contains the global position system (GPS) and the navigation module.

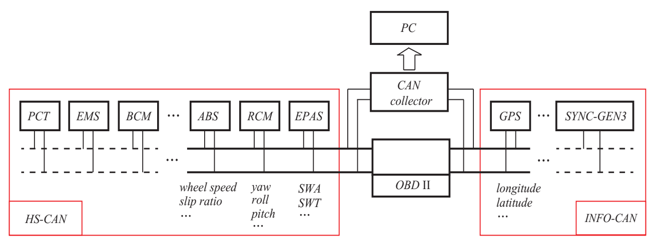

Fig. 4. Illustration of the CAN network on MKS.

The collected data include the steering wheel angle, the steering column torque, the yaw rate, the longitude and the latitude of the vehicle, where the signals of the steering wheel angle and the steering column torque are provided by the electric power assisted steering (EPAS), the yaw rate is provided by the restraint control module (RCM) and the position information is provided by the GPS system. The CAN bus network of the MKS is summarized in Fig. 4. The setups of the test conditions for the SHC are summarized in Table I.

V. Results and Analysis

The data from the test were processed by applying the joint E-/UKF and the dual E-/UKF to estimate the parameters of the driver model. Since the road curvature and the side slip angle of the vehicle were not directly measured, we first obtain these missing necessary values by processing the GPS data [18]. Fig. 5 shows the trajectory of the vehicle in the Earth-bound West/South frame.

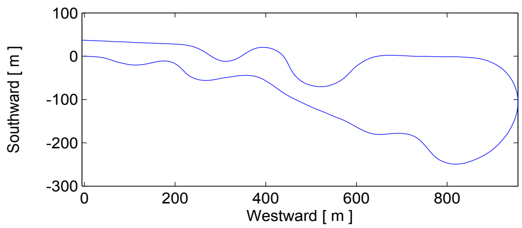

Fig. 5. Trajectory of the vehicle in the SHC test.

The side slip angle and the road curvature are estimat based on the trajectory of the vehicle and are given by Fig.

A. Driver Parameter Identification

This section shows the results of the identified driver p rameters. We processed the field test data using the joint EK the joint UKF, the dual EKF and the dual UKF separately, that we can compare the identified driver parameters obtain from different methods. We took the same set of data fro the SHC tests as used to obtain the Fig. 5-6. In every sing implementation, we use the first 60% of data for the paramet training and use the remaining 40% of data for the validatic

By designing the appropriate Kalman filter parameters, su as the process noise covariance, the measure noise covarian and the initial state covariance matrix, we obtain reasonable estimation for the parameters. The process noise covariance is considered to be the most critical and therefore has to be carefully tuned. Fig. 7 illustrates the steering wheel torque from data, the training curve of the Kalman filter and the simulated output corresponding to the identified model parameters. The green plots in Fig. 7 show how the prediction of the steering wheel torque at the current time step agrees with the current data. After about 1 minute or so the prediction results get stabilized and agree well with data. The trajectories of the estimated states (we only show the driver parameters, and each parameter is scaled such that the initial value is one) corresponding to the joint EKF are given in Fig. 8. The red plots in Fig. 7, which are drawn to validate the identified driver parameters, are very close and they agree well with data. Although one sees some difference between the validation plots and data, the results are reasonable, since the parameters of the real driver may change with time. The identified parameters are given in Table II.

TABLE I
STEERING HANDLING COURSE (CONSTANT VELOCITY).

Speed [mph]	Novice	Expert	Racing
30	1 lane, unsmooth	1 lane, smooth	2 lanes, smooth
45	1 lane, unsmooth	1 lane, smooth	2 lanes, smooth

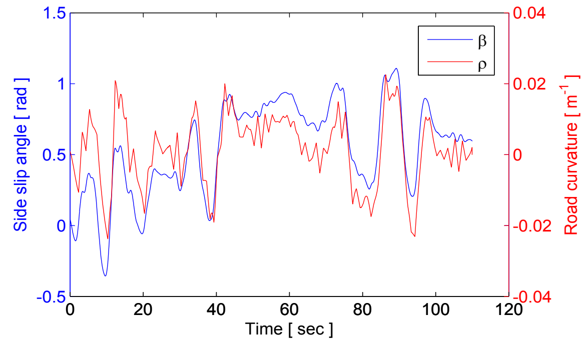

Fig. 6. The side slip angle and the road curvature in the SHC test.

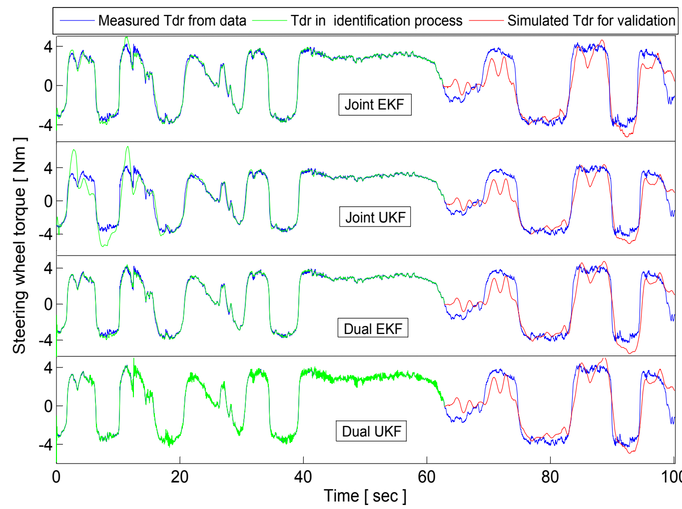

Fig. 7. The data, the training curve and the simulated curve from the Joint/Dual E-/UKF.

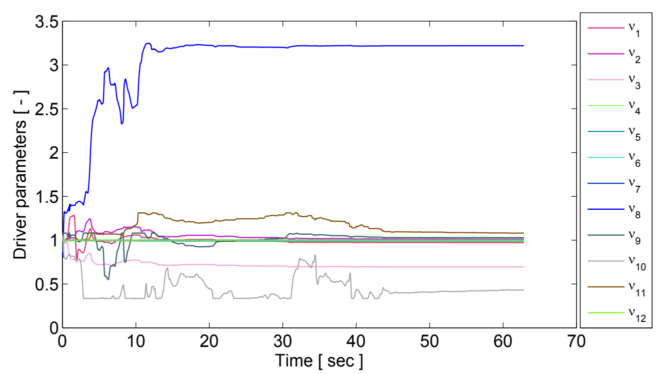

Fig. 8. The trajectories of the driver parameters during the training process.

Based on these results, we refined the model by assuming the process noise for the vector ν is colored and letting

$$\dot{\nu} = \zeta, \qquad \dot{\zeta} = \xi, \tag{13}$$

where ζ and ξ are the process noise. The equations in (13) drive the parameter vector to change with time. We implement the Kalman filfter again (i.e., the joint UKF) and record the

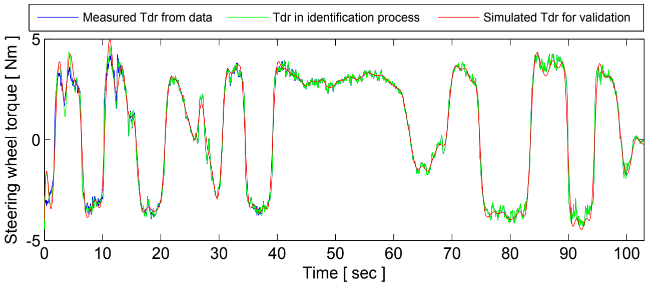

Fig. 9. The data, the training curve and the simulated curve from the Joint UKF.

TABLE II
DRIVER MODEL PARAMETERS; (JEKF=JOINT EKF, DEKF=DUAL EKF, UB=UPPER BOUND, LB=LOWER BOUND)

Parameter	JEKF	JUKF	DEKF	DUKF	UB	LB
K_a	22.10	21.62	21.29	21.29	100	5
K_c	149.87	152.35	151.88	150.96	200	5
T_L [sec]	0.33	0.34	0.33	0.33	5	0
T_I [sec]	0.26	0.26	0.26	0.26	0.5	0
T_N [sec]	0.18	0.19	0.19	0.20	0.3	0.01
t_p [sec]	0.11	0.11	0.11	0.11	0.5	0.01
ℓ_s [m]	12.06	12.16	12.25	12.07	15	3
K_D [m]	0.37	0.27	0.11	0.31	1.5	0.1
K_G [m]	-0.74	-0.64	-0.79	-0.43	-0.4	-1.5
T_{k_1} [m]	1.50	1.54	1.97	1.57	6	1
T_{k_2} [m]	3.82	3.71	3.42	3.81	6	1
T_{k_3} [m]	0.01	0.01	0.01	0.01	0.03	0.01

estimates for the driver parameters at each time step, and then we perform the simulation with the time-varying driver parameters (see Fig. 9). Fig. 9 indicates that the parameterized driver model with time-varying parameters can characterize the driver's steering behavior more accurately. Due to the lack of space, we only show how the driver parameter K_c changes with time in Fig. 10.

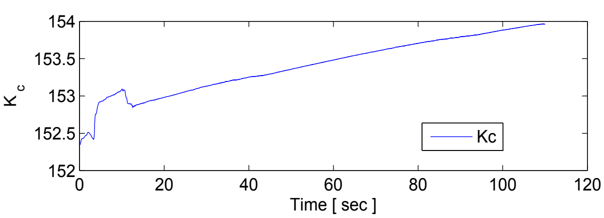

Fig. 10. The trajectory of K_c during the training process.

VI. CONCLUSIONS

This paper adopts the parameterized two-point visual driver model to characterize the steering behavior of the driver and conducts field tests to validate the model. We have separately implemented the joint EKF, the joint UKF, the dual EKF and the dual UKF to estimate the parameters based on field test data conducted at Ford's Dearborn Development Center (DDC) test facility. The validation results agree well with the data. All four versions of Kalman filters used in this paper show close estimation results. The UKF is considered to be more accurate than the EKF in propagating the Gaussian random variables, but the difference was not obvious in this work. The Kalman filter parameters, especially the process noise coviarance, must be well tuned or appropriately chosen in order to obtain good results. The results of our investigation indicate that the driver parameters are not exactly constant, but they rather vary slowly during a driving task more that few minutes long. The next step would be to analyze how the driver parameters change under different test conditions, and further categorize the drivers into different groups based on these identified driver parameters.

ACKNOWLEDGMENT

This work is supported by National Science Foundation awards CMMI-1234286 and CPS-1544814 and the Ford Motor Company. The authors acknowledge the excellent work done in the field test by Mr. Dave Starr from Ford Motor Company.

REFERENCES

[1] A. Gray, M. Ali, Y. Gao, J. Hedrick, and F. Borrelli, "Semi-autonomous vehicle control for road departure and obstacle avoidance," *IFAC Control of Transportation Systems*, pp. 1–6, 2012.

[2] S. Noth, I. Rañó, and G. Schöner, "Investigating human lane keeping through a simulated driver," in *Proceedings of the Driver Simulation Conference*, Paris, France, September 6-7, 2012.

[3] D. H. Weir and D. T. McRuer, "Measurement and interpretation of driver steering behavior and performance," SAE Technical Paper, Tech. Rep., February 1973.

[4] R. Hess and A. Modjtahedzadeh, "A control theoretic model of driver steering behavior," *IEEE Control Systems Magazine*, vol. 10, no. 5, pp. 3–8, 1990.

[5] A. Burgett and R. Miller, "Using parameter optimization to characterize driver's performance in rear end driving scenarios," in *Proceedings: International Technical Conference on the Enhanced Safety of Vehicles*, vol. 2003. Nagoya, Japan: National Highway Traffic Safety Administration, May 19-22, 2003, p. 21.

[6] M. Flad, C. Trautmann, G. Diehm, and S. Hohmann, "Individual driver modeling via optimal selection of steering primitives," in *World Congress*, vol. 19, no. 1, Cape Town, South Africa, August 24-29, 2014, pp. 6276–6282.

[7] C. Sentouh, P. Chevrel, F. Mars, and F. Claveau, "A sensorimotor driver model for steering control," in *IEEE International Conference on Systems, Man and Cybernetics*, San Antonio, TX, October 11-14, 2009, pp. 2462–2467.

[8] E. Donges, "A two-level model of driver steering behavior," *Human Factors: The Journal of the Human Factors and Ergonomics Society*, vol. 20, no. 6, pp. 691–707, 1978.

[9] M. F. Land and D. N. Lee, "Where do we look when we steer." *Nature*, vol. 369, no. 6483, pp. 742–744, 1994.

[10] D. D. Salvucci and R. Gray, "A two-point visual control model of steering," *Perception*, vol. 33, no. 10, pp. 1233–1248, 2004.

[11] H. Neumann and B. Deml, "The two-point visual control model of steering – new empirical evidence," in *Digital Human Modeling*. Springer, 2011, pp. 493–502.

[12] E. A. Wan and R. Van Der Merwe, "The unscented Kalman filter for nonlinear estimation," in *Adaptive Systems for Signal Processing, Communications, and Control Symposium*, Alberta, Canada, October 1-4, 2000, pp. 153–158.

[13] S. Zafeiropoulos and P. Tsiotras, "Design of a lane-tracking driver steering assist system and its interaction with a two-point visual driver model," in *American Control Conference*, Portland, OR, June 4-6, 2014, pp. 3911–3917.

[14] D. Simon and T. L. Chia, "Kalman filtering with state equality constraints," *IEEE Transactions on Aerospace and Electronic Systems*, vol. 38, no. 1, pp. 128–136, 2002.

[15] S. Ko and R. R. Bitmead, "State estimation for linear systems with state equality constraints," *Automatica*, vol. 43, no. 8, pp. 1363–1368, 2007.

[16] C. Yang and E. Blasch, "Kalman filtering with nonlinear state constraints," *IEEE Transactions on Aerospace and Electronic Systems*, vol. 45, no. 1, pp. 70–84, 2009.

[17] B. O. S. Teixeira, L. A. Tôrres, L. A. Aguirre, D. S. Bernstein, *et al.*, "Unscented filtering for interval-constrained nonlinear systems." in *Proceedings of the IEEE Conference on Decision and Control*, Canxun, Mexico, December 9-11, 2008, pp. 5116–5121.

[18] S. P. Drake, "Converting GPS coordinates [ϕ, λ, h] to navigation coordinates (ENU), Tech. Rep. DSTO-TN-0432, April 2002.